CMS Note 2001/034

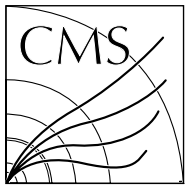

The Compact Muon Solenoid Experiment

CMS Note

Mailing address: CMS CERN, CH-1211 GENEVA 23, Switzerland

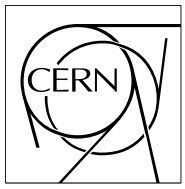

June 22nd, 2001

Electron Reconstruction in the CMS Electromagnetic Calorimeter

E. Meschi[1], T. Monteiro[1], C. Seez[2] and P. Vikas[3]

Abstract

This note describes the reconstruction of electrons using the electromagnetic calorimeter (ECAL) alone. This represents the first step in the High Level Trigger reconstruction and selection chain. By making “super-clusters” (i.e. clusters of clusters) much of the energy radiated by bremsstrahlung in the tracker material can be recovered. Representative performance figures for energy and position resolution in the barrel are given.

1. CERN, Geneva
2. Imperial College, London
3. Univ. of Minnesota, Minneapolis

1 Introduction

The first step in the reconstruction of an electron, as currently envisaged in the development of reconstruction algorithms in the context of the CMS High Level Trigger, is the clustering of the energy deposits in the electromagnetic calorimeter (ECAL) and the estimation of the electron's energy and position from this information. In the barrel section this involves the energy deposited in the lead tungstate crystals alone, in the endcap energy is also deposited in the ~$3X_0$ thick preshower detector. The structure of the ECAL, as simulated for these studies, differs little from the extensive description given in ref. [1].

We concentrate first on *electron* reconstruction because the target transverse momentum cuts and thresholds for triggering on electrons are much lower than those for photons. We are interested here in electrons in the range $10 < p_T < 40$ GeV. We expect, and have loosely verified, that single and double photons, at the significantly higher transverse momenta at which we will wish to preserve them, will be adequately reconstructed by our electron algorithms to pass the Level-2 trigger.

Electrons radiate in the material between the interaction point and the ECAL. The bending of the electron in the 4T magnetic field results in a spray of energy reaching the ECAL. The spreading of this spray is, to good approximation, only in the φ-direction. The electron energy can be collected by making a cluster of clusters along a φ road. We call this cluster of clusters a *super-cluster*.

The studies outlined in this note have been carried out using simulated data produced by full GEANT [2] simulation of the CMS detector, and ORCA [3] simulation of the digitization involving, where appropriate, the addition of pileup events from many bunch-crossings.

2 Clustering

The collection of energy resulting from an electromagnetic shower in a fine grained crystal calorimeter can be approached as a pattern recognition procedure. The shower should appear as a local maximum (bump) in a spacial array of crystal energy deposits. The search for such bumps starts by looking for single crystal local maxima ("seeds"), which are then extended to collect as large a fraction of the original shower energy deposition as possible, while avoiding the collection of energy depositions from nearby particles and noise. Using the currently simulated data the situation is complicated by a noise suppression algorithm which is applied, at digitization, to reduce the volume of data stored. A threshold on crystal energies is applied. The current thresholds are 60 MeV in the barrel, and 300 MeV in the endcap. As a result bumps due to electromagnetic showers are subject to two effects which can deteriorate the energy resolution: 1) the bump is split or 2) the bump is cut off before the shower edges due to noise suppression or noise fluctuations.

In the case of a non-converting photon shower, for example, the bump should ideally map the shower shape almost perfectly. However, at the shower borders, where energy depositions are comparable to noise, energy belonging to the shower may be noise-suppressed, or a large noise fluctuation may fake the presence of a secondary bump. This has suggested in the past that the collection of energy in a fixed array of crystals around a seed may be less prone to this kind of problem, and therefore yield a better energy resolution than any bump-finding procedure. Indeed, such a fixed window algorithm provides to date the best energy resolution for non-converting photons. However, quite apart from other considerations which might be raised concerning the desirability or otherwise of fixed windows, electrons radiate bremsstrahlung photons which are spread over a region in the calorimeter which may be much larger than that occupied by a single shower. This necessitates a more complex and flexible clustering of energy deposits.

3 The Island algorithm

The island algorithm starts by a search for seeds. Seeds are defined as crystals with an energy above a certain threshold. This threshold is currently defined on transverse energy. A list of seeds is prepared and ordered in decreasing energy. The algorithm then loops over seeds and removes those seeds that are adjacent to higher energy ones.

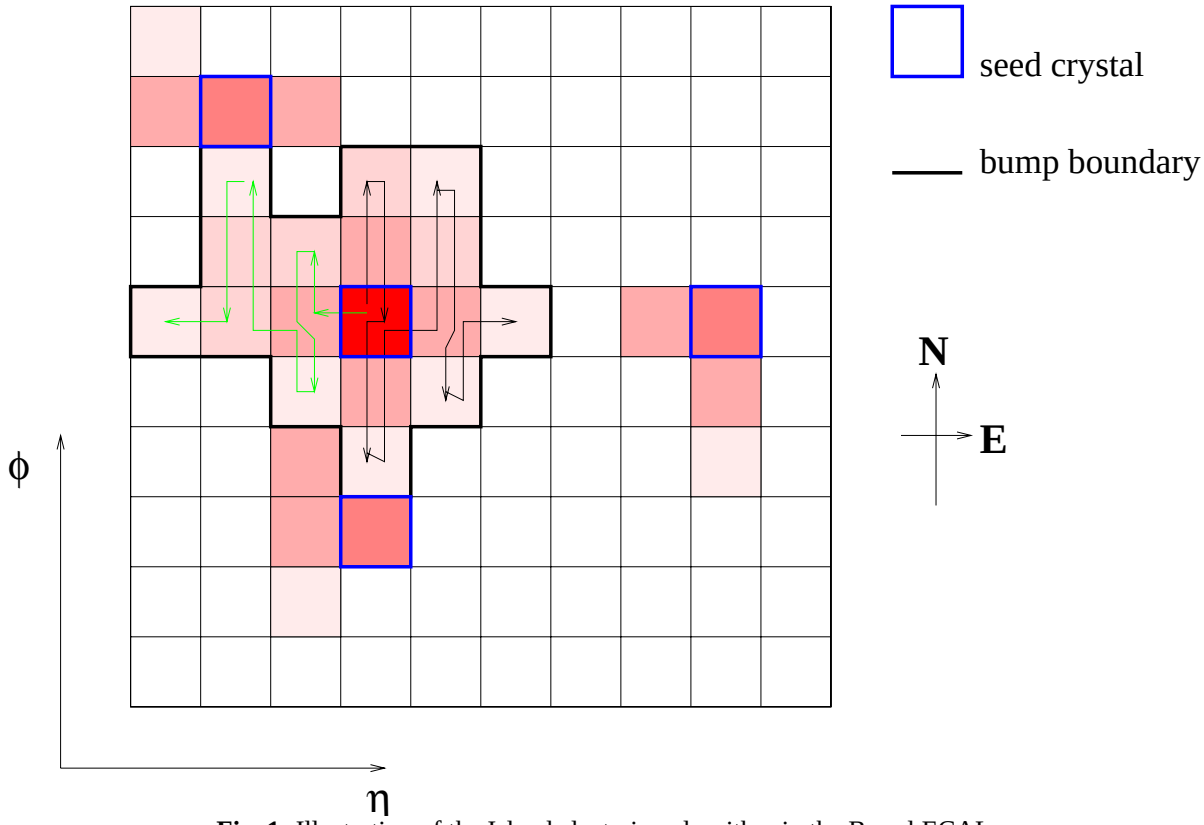

Fig. 1: Illustration of the Island clustering algorithm in the Barrel ECAL

Starting from the most energetic seed, the algorithm collects crystals belonging to a certain cluster. The sequence is sketched in Fig. 1: starting from the seed position, the algorithm moves in both directions in φ and collects all crystals until it sees a rise in the energy, or a hole[4]. The possibility of a 'hole' exists because of the zero-suppression currently applied to the simulated data production. The algorithm then moves one step in η and makes another φ search. The η-steps are stopped when a rise in energy, or a hole, is encountered. When one direction in η is completed, the algorithm goes back to the seed position and works in the other η direction. All the collected crystals are marked as belonging to that one cluster and cannot be used anymore. If a seed is included in one cluster it cannot subsequently be used to seed another. This procedure guarantees that there is no double counting of crystal energy. The algorithm has the following features: 1) it will not split two showers due to an

4. The elegance of defining a cluster in this way, as a series of connected crystals containing energy deposits which decrease monotonically from a seed crystal, has a price: single crystals can be split off from the main cluster because of a noise fluctuation. In the endcap, where this algorithm is used for electron showers, the struggle to improve the energy resolution will probably necessitate a mechanism to reattach these orphan crystals — for example, by applying a threshold on the rise required to stop the clustering.

electron and a radiated soft photon if the two showers are close enough; 2) it will split two showers coming from the two legs of a π^0 decay if the opening angle is sufficiently large; 3) energy deposited in crystals below the seed threshold may remain unclustered: this energy loss may be significant, depending on the seed threshold, on the other hand, small deposits of energy due to noisy hits or low-energy particles from pileup events will not be clustered either.

The seed threshold E_T is the only parameter of the island algorithm. The value of this threshold has to be a trade-off between cutting off noisy hits and low-energy pileup, thus also keeping the execution time low, and an optimal energy resolution.

The capability of doing standalone reconstruction of e.g. π^0 decays is an interesting feature of the island algorithm. In the barrel ECAL, this is illustrated by the plot in Figure 2. For a sample of p_T = 15 GeV π^0s in the barrel fiducial volume the cluster positions are calculated using the procedure outlined in section 8. The 4-momenta are extracted from the energy measurement and the invariant mass is calculated, correcting for the primary vertex position in z. The resulting distribution for the 15 GeV sample is nicely peaked at 140 MeV. In the plot the actual mass scale is arbitrary, since the energy scale has not been set. Approximately 40% of the fiducial π^0s are reconstructed. Interestingly, the energy split between the two close clusters assumed to be the two legs of the decay seems to be correct, though for increasing particle p_T, the opening angle becomes too small for the two legs to be separated in the ECAL, and the energy splitting poorer, generating peaks at higher mass values.

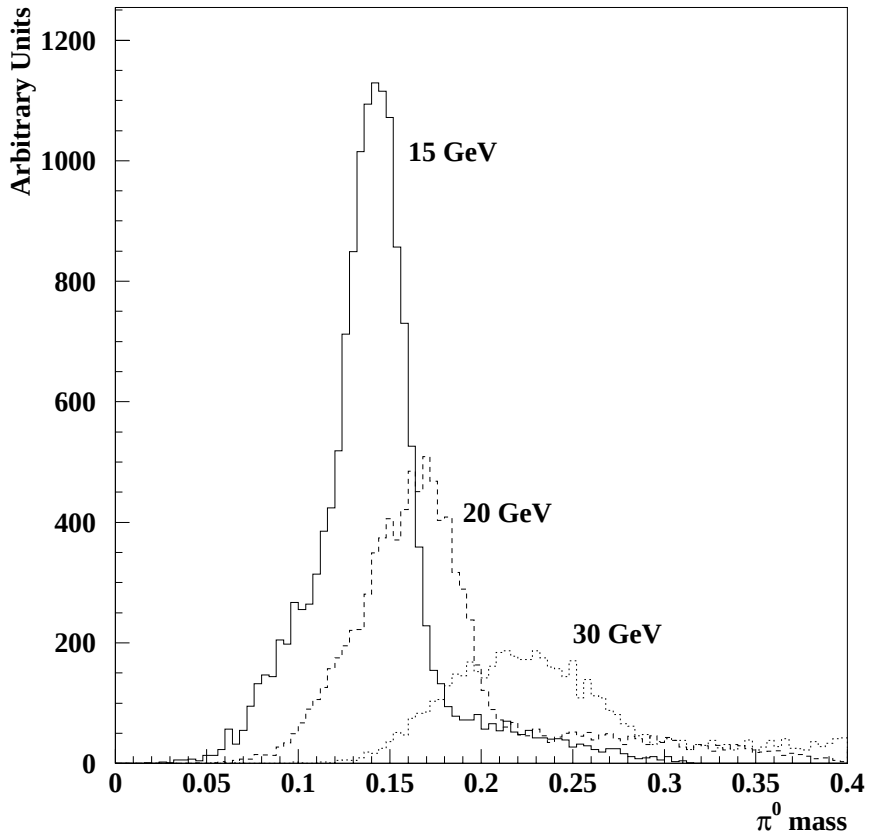

Fig. 2: Standalone reconstruction of single $\pi^0 \rightarrow \gamma\gamma$ using island clusters for different π^0 p_T

4 Bremsstrahlung

The information currently stored in the GEANT detector simulation step can be used to look at the characteristics of electrons. For example, electrons in the barrel, p_T = 35 GeV, $|\eta| < 1.5$, simulated with the CMS120 geometry, are found to have a mean energy loss of 43.6% before exiting the tracker volume[5]. This corresponds to an average material thickness of $0.57X_0$, since 43.6% = 1 -exp(-0.57). Most of the energy is radiated as low energy photons. This is illustrated in Figure 3.

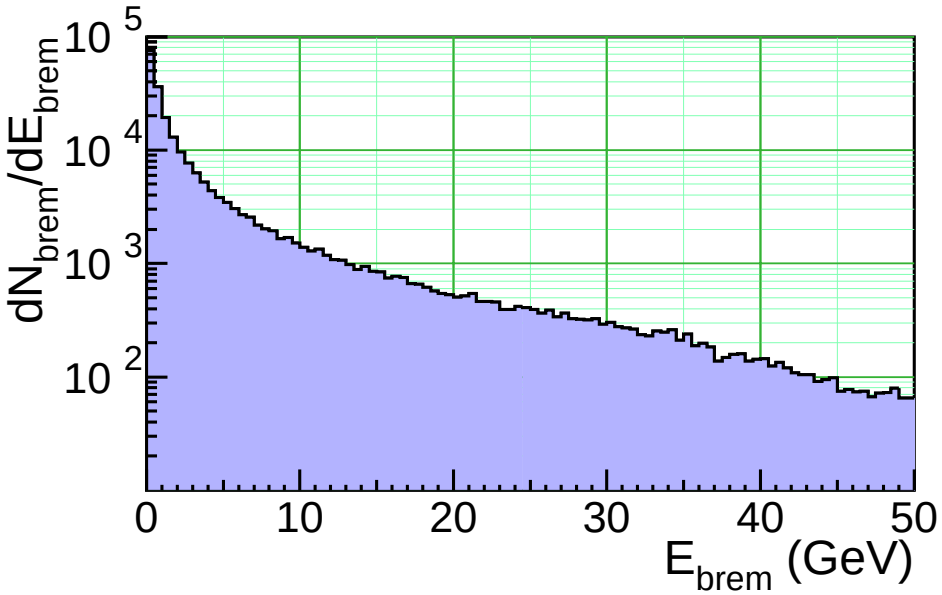

Fig. 3: Energy spectrum of bremsstrahlung photons emitted in the tracker material by p_T = 30 GeV, $|\eta| < 1.5$ electrons

Many of the low energy radiated photons fall within the main calorimeter cluster, but the large fraction of energy radiated by electrons means that the energy reaching the calorimeter can be spread by distances of many crystals and may be split from the main cluster. To good approximation this energy reaches the calorimeter along a line in φ (i.e. with constant η).

5 Clusters of Clusters

A possible approach to recollecting energy radiated by an electron that falls outside the main shower cluster is to build a cluster of clusters. In much the same way as energy is clustered at the level of calorimeter cells, non-overlapping clusters can in turn be clustered into calorimetric "super-clusters". The procedure is seeded by searching for the most energetic cluster and then by recollecting the others based on some geometric criterion, e.g. a fixed search area around the seed position. In a purely axial magnetic field the clusters belonging to radiation from a single electron will be nicely aligned in η, but spread in ϕ, as illustrated in Figure 4 left. In this case, one can hope that collecting all the clusters in a narrow η window, whose size is dictated by the η position resolution of the detector, it is possible to recover most of the radiated energy (at least all that is clustered), as illustrated in the right side of Figure 4. Such a procedure, applied to single electrons reconstructed using the

5. Strictly speaking, only bremsstrahlung photons with E > 100 MeV are recorded and included in the figures given.

island clustering algorithm, considerably reduces the tails in the reconstructed energy distribution, as illustrated in Figure 5.

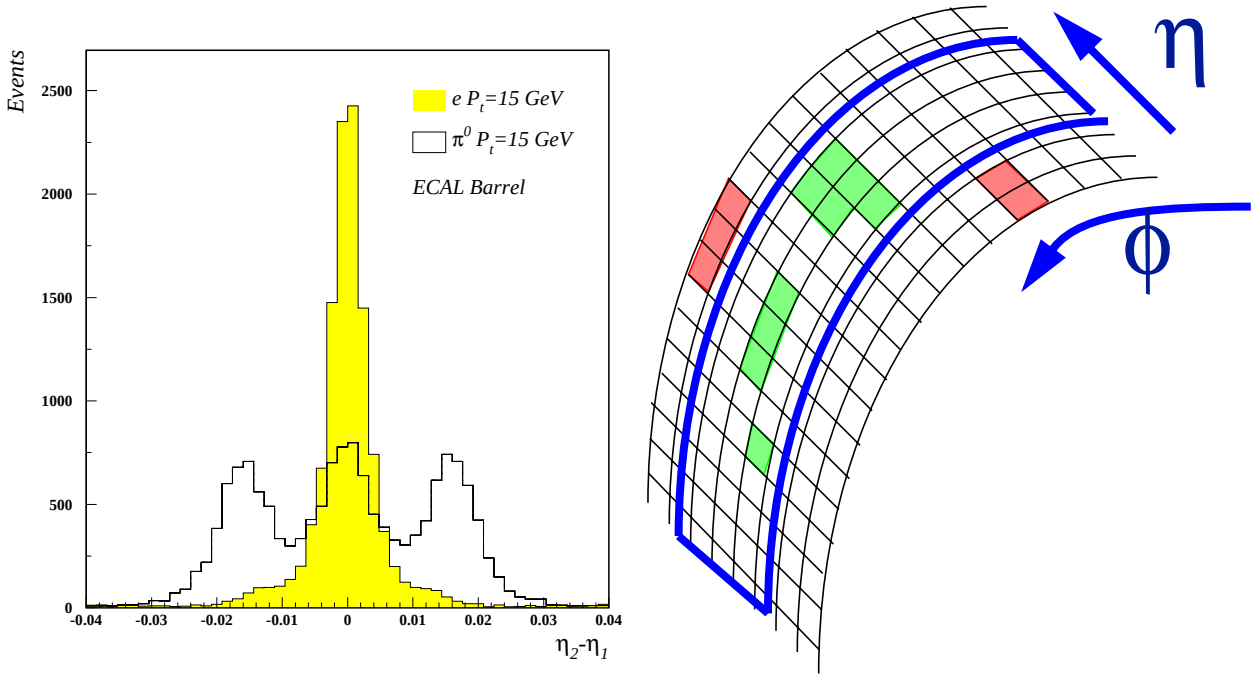

Fig. 4: The closest cluster to a single electron most energetic island cluster lies in a very narrow η slice, as opposed to the single π^0 case. The plot on the left shows the η_2-η_1 distribution for single electrons and π^0s. A super-cluster algorithm (right) collects all calorimetric clusters satisfying a given geometric condition (e.g. lying in a certain region around the "main" cluster) into a collection of clusters

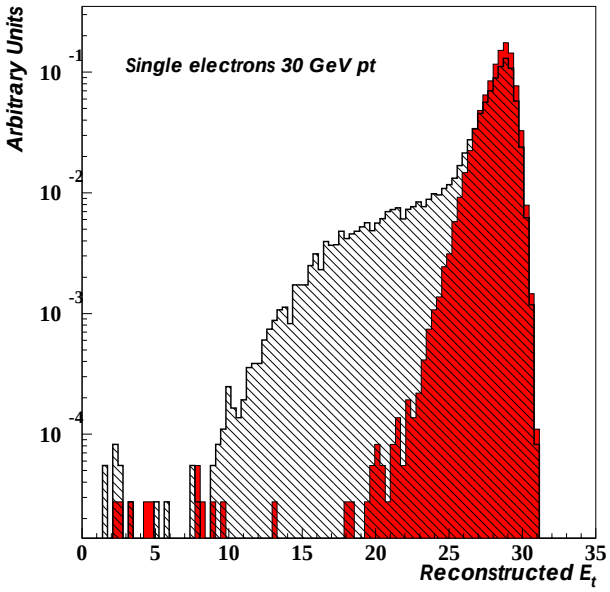

Fig. 5: Reconstructed transverse energy for 30 GeV p_T electrons using a single island cluster (hatched) and a super-cluster collected in a 1-crystal-wide window in η around it (solid filled).

6 The Hybrid algorithm

It has already been mentioned that for single showers, such as those produced by unconverted photons, or those produced by electrons in testbeam conditions, energy sums of fixed arrays of crystals seem to consistently give better results in terms of energy resolution, than energy sums of crystals collected dynamically according to a cluster or "bump" finding algorithm. This seems to be because containment variation as a function of impact position is amplified by dynamic cluster finding. The Hybrid algorithm attempts to use the $\eta-\varphi$ geometry of the barrel crystals to exploit the knowledge of the lateral shower shape in the η direction (taking a fixed domino of three or five crystals in η), while searching dynamically for separated (bremsstrahlung) energy in the φ direction.

A clarification is perhaps useful for users of the software: the Hybrid algorithm is inherently a *super*-clustering algorithm. The software framework in the ElectronPhoton domain has been set up as a three step process: 1) make clusters, using a clustering algorithm, 2) promote clusters passing some criteria to the status of 'seed clusters', 3) make super-clusters by associating other clusters to seed clusters. The Hybrid algorithm has been fitted into this framework, but its seed making and super-clustering steps in this framework associate sub-clusters that have, in fact, already been covertly associated during the first clustering step. The Hybrid algorithm is designed to reconstruct relatively high energy electrons in the barrel (so far we have used it for electrons with $p_T > 10$ GeV). By contrast, when looking for small deposits of energy in individual clusters, for example when making a calorimetric isolation cut, the basic clusters of the Island algorithm are more appropriate objects to work with.

Starting from a seed crystal — the maximum energy crystal in the region being searched, which must also satisfy the condition $E_T > E_T^{hybseed}$ — 1x3 crystal dominoes are made, each with their central crystal aligned in η with the seed crystal. If the energy of the central crystal of a domino is greater than E_{wing} then a 1x5 domino is used. This making of dominoes proceeds N_{step} crystals in each direction from the original seed. Dominoes with energy less than E_{thresh} are eliminated. The domino construction step of the algorithm is illustrated in Figure 6.

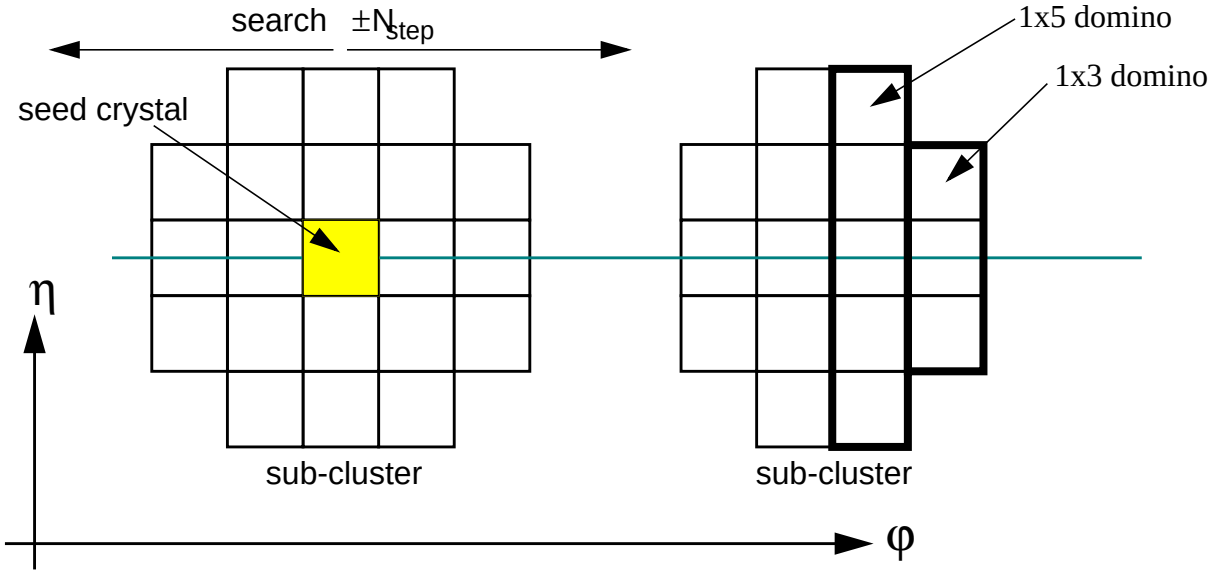

Fig. 6: Domino construction step of Hybrid algorithm

The dominoes are then clustered in φ. Each distinct cluster of dominoes is required to have a seed domino with energy greater than E_{seed}. We thus end up with a cluster of clusters, entirely analogous to super-clusters of Island clusters. The default values of the control parameters are shown in Table 1.

Table 1: Default values of control parameters for Hybrid algorithm

Parameter description	label used in text	default value
Minimum E_T for Hybrid super-cluster seed crystal	$E_T^{hybseed}$	1 GeV
Number steps (crystals) for search in φ (in each direction)	N_{step}	10
Threshold for using 1x5 crystals (rather than 1x3)	E_{wing}	1 GeV
Threshold for using domino	E_{thresh}	0.1 GeV
Minimum domino to make a disconnected subcluster	E_{seed}	0.35 GeV

7 Endcap reconstruction with the preshower

Much of the endcap is covered by a preshower device with two planes of silicon strip readout. The energy deposited in the preshower detector (which is about 3 X_0 thick) needs to be added to the crystal clusters. The constants relating the energy deposited in the two planes of silicon to the crystal energy are explained in ref [4].

The crystal energy is clustered using the Island algorithm and the clusters are associated to form super-clusters, then a preshower cluster is constructed in each plane, in front of each crystal cluster of the super-cluster. The search area in the preshower is centred on the point determined by extrapolating the crystal cluster position to the preshower plane in the direction of the nominal vertex position.

The energy resolution for electrons found after using this reconstruction procedure is significantly worse, by a factor of about two, than that obtained for electrons of the same p_T in the barrel. By contrast, the energy resolution for unconverted photons with a flat p_T spectrum ($25 < p_T < 50$ GeV), using a fixed window 3x3 crystal algorithm, is, to good approximation, the same in the endcap as it is in the barrel ($\sigma_{eff}/E < 0.9\%$[6], this is also consistent with earlier results given in ref [1]) — the degradation caused by the larger electronics noise (150 MeV per crystal) and the preshower sampling being compensated by the higher energies in the endcap. Also, the fraction of the incident energy reconstructed varies as a function of η. Four factors which contribute to these problems have been identified. They are given here in approximately the order of importance that they currently appear to have:

1. The default magnitude of the Island clustering algorithm seed threshold (E_T = 500 MeV) results in the loss of some small bremsstrahlung clusters. Lowering the threshold improves the energy resolution, but there is, at present, a conflict with the need to avoid making too many small clusters.
2. Only a single preshower cluster in each plane is matched to each crystal cluster.

6. We define σ_{eff} as the half-width containing 68.3% of the distribution — see section 10.

3. The zero suppression threshold used in the data simulation production is set to 300 MeV in the endcap crystals (twice the noise width). This seems to result in large fluctuations in the fraction of energy clustered. Because of this zero suppression the fraction of energy clustered also depends on the shower energy.
4. The response of the preshower and endcap crystal system to very low energy bremsstrahlung photons (E ~ 2 GeV) is not precisely proportional to its response to high energy showers.

It is hoped and expected that an improved endcap electron reconstruction procedure will be available before the end of the year.

8 Position measurement using log weighting technique

A simple position measurement of the shower can be obtained by calculating the energy weighted mean position of the crystals in the cluster. Going beyond this simple picture, two issues need to be considered in more detail.

Firstly, the meaning of *crystal position* needs to be defined. The crystals in the CMS ECAL are quasi-projective, and do not exactly point to the nominal interaction vertex. So the lateral position (η,φ) of the crystal axis depends on depth as illustrated in Fig. 7. A depth *tmax* thus needs to be defined. This depth is something like the longitudinal centre of gravity of the shower, and its optimal mean value varies logarithmically with the shower energy. There is also a dependence on particle type — electron showers have a maximum about one radiation length less deep than photon showers. In the position measurement used for both Island and Hybrid super-clusters the depth is measured from the front face of the crystals along the direction from the nominal vertex position to the approximate shower position calculated using the arithmetic energy weighted mean of the shower front face centres.

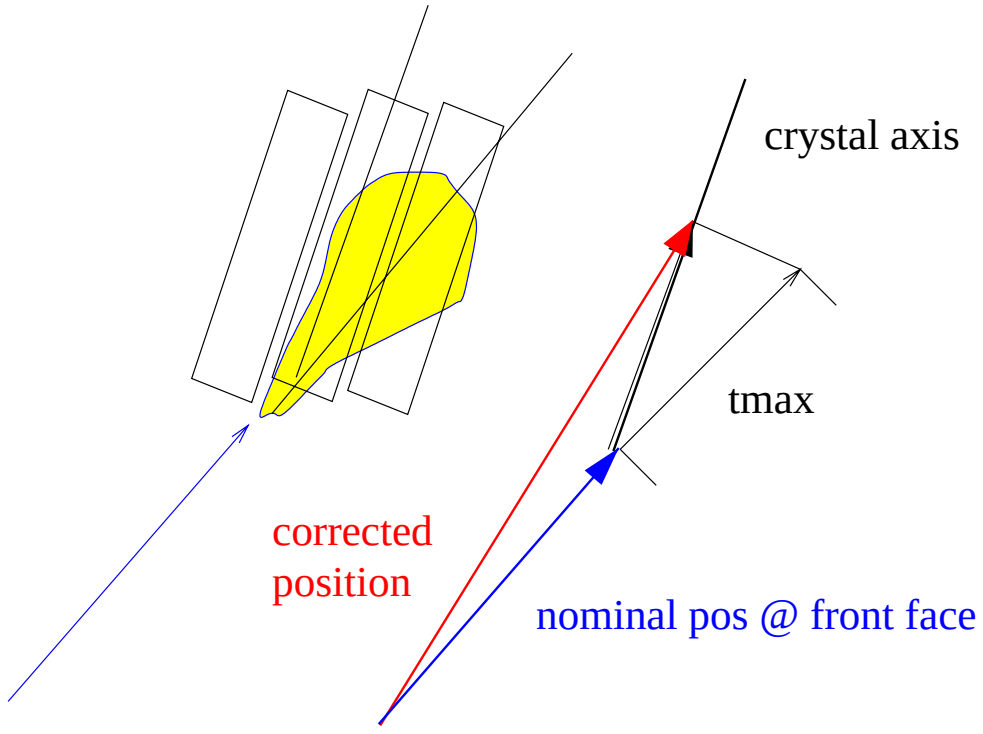

Fig. 7: Illustration of the crystal offpointing

To account for the energy dependence a parametrization is used: A(B + log(E)). The dependence of the shower maximum on energy is given approximately by log(E/GeV) X_0. This approximation works well for lead tungstate [5], so the variable A is set to the radiation length of lead tungstate (0.89cm), and this seems to reproduce the depth dependance adequately in the relatively small energy range over which we have used it. For best performance with electrons, B is set to 5.7 in the absence of the preshower detector, and 2.0 when the preshower detector is present. These values are most reliably obtained by looking at the zero offsets (i.e. the difference between the measured and the true position) in η separately in the two halves of the detector — η is used rather than φ to avoid any possible confusion with the bending in the field (although equal use of e^+ and e^- also eliminates this problem), and the two halves of the detector must be examined separately because the offpointing angles are reversed. Figure 8 illustrates the technique. Another possible technique is to minimize the position resolution in η, in each half of the detector, which is smeared by the varying offpointing angle due to the spread of the z-vertex position.

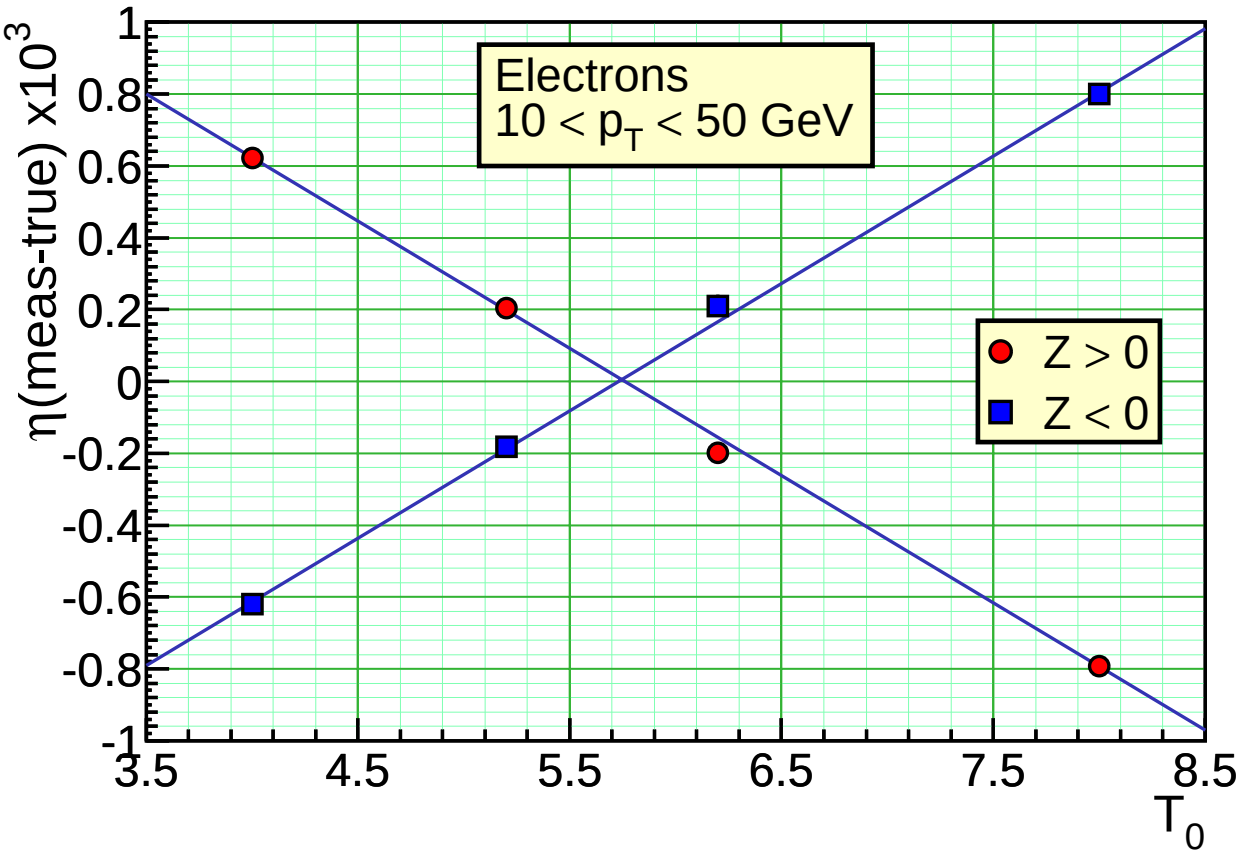

Fig. 8: Mean of difference between measured and true position (in η) versus B, shown for each half of the barrel separately, for electrons with a flat p_T spectrum in the range 10-50 GeV. The difference is shown as a function of our parameter B (T_0 in the plot) with A=0.89cm.

The second issue that requires more detailed treatment is related to the lateral shower shape. Since the energy density does not fall away linearly with distance from the shower axis, but rather

exponentially, a simple energy weighted mean of crystal energies is distorted and the measured position is biased towards the centre of the crystal containing the largest energy deposit (see Fig. 9).

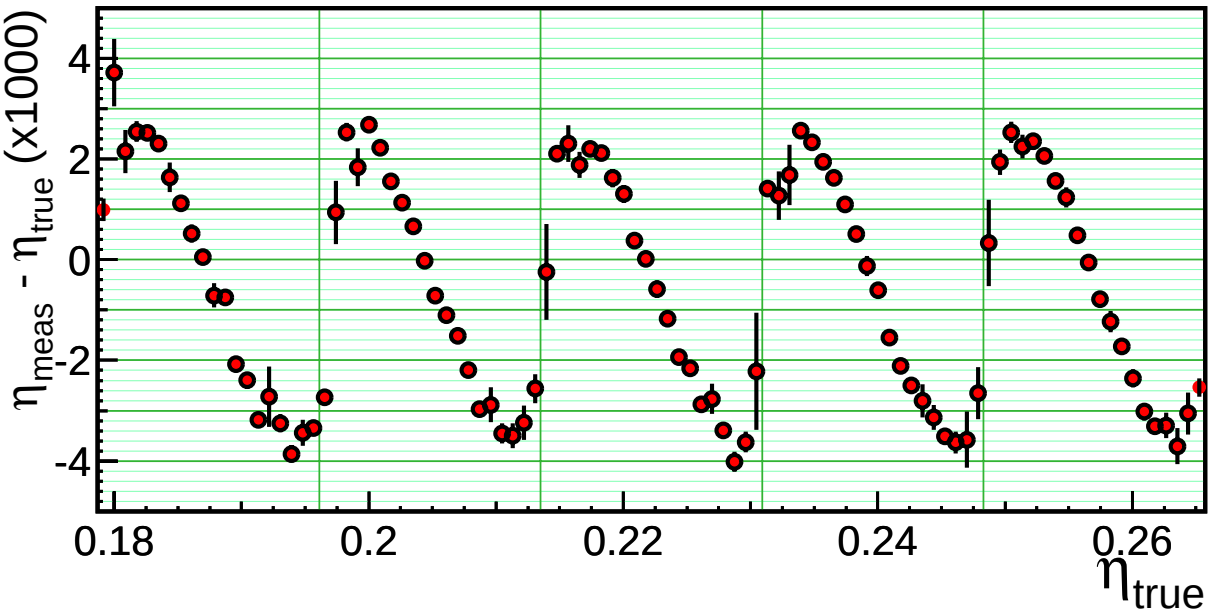

Fig. 9: S-shape. The plot shows the difference between the reconstructed and true η for island clusters calculated as the linear weighted center-of-gravity, for electrons $10 < p_T < 50$ GeV, over a range of five crystals in the barrel. The vertical lines represent the approximate crystal boundaries at a depth of 8.1 cm.

In earlier studies position corrections were applied to remove this bias (the so-called S-shape correction [6]), but we now use a simpler algorithm which delivers almost as good precision by calculating the weighted mean using the logarithm of the crystal energy:

$$x = \frac{\sum x_i \bullet W_i}{\sum W_i}$$

where x_i the position of crystal i, and W_i is the log weight of the crystal — the log of the fraction of the cluster energy contained in the crystal, calculated with the formula:

$$W_i = W_0 + \log\left(\frac{E_i}{\sum E_j}\right)$$

where the weight is constrained to be positive, or is otherwise set to zero. W_0 then controls the smallest fractional energy that a crystal can have and still contribute to the position measurement. Its default value, obtained after optimization studies, is 4.2 — so that crystals in the cluster containing more than 1.5% of the cluster energy contribute to the position measurement [7]. The resulting systematic error on the reconstructed position is shown in Fig. 10.

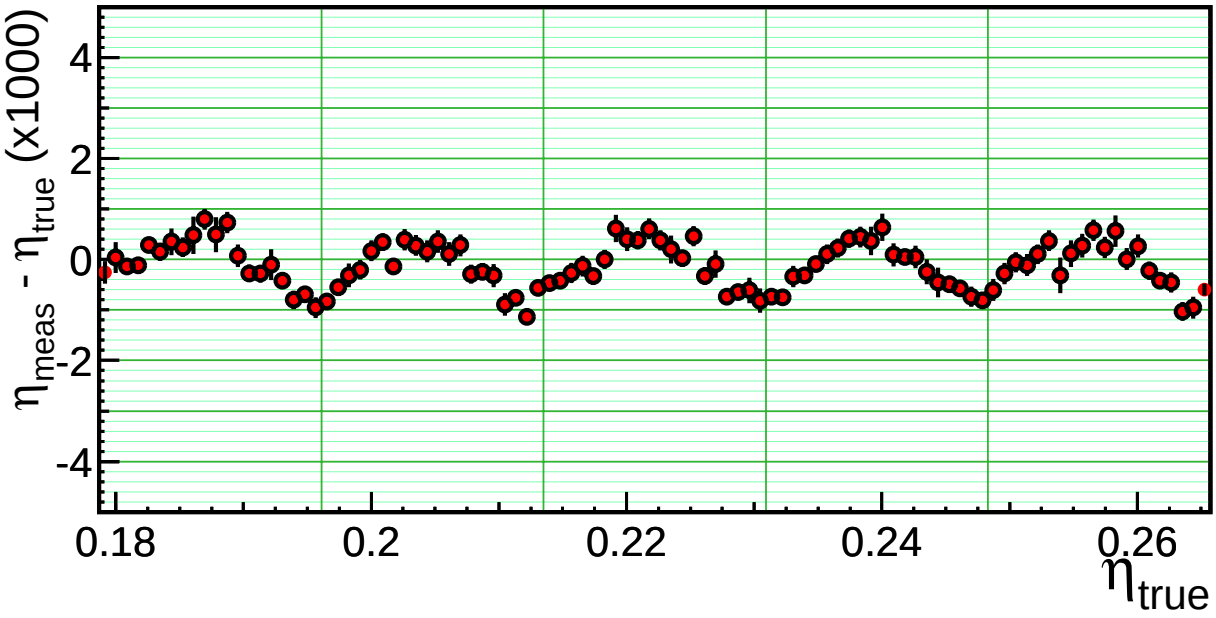

Fig. 10: Systematic error on reconstructing η of the cluster when using a log-weighting center of gravity, for electrons $10 < p_T < 50$ GeV, over a range of five crystals in the barrel. The vertical lines represent the approximate crystal boundaries. (cf. Fig. 9).

9 Energy measurement and energy scale corrections

The measurement of energy in the crystals is obtained by simple addition of the deposits measured in the crystals — although more complex estimators have been envisaged [8].

Even in the areas not covered by the preshower detector the energy containment of the clustered crystals is not complete. The reconstructed energy distribution, E_{meas}/E_{true}, shows a peak at a few percent less than unity, and a long tail on the low side due to unrecovered bremsstrahlung energy. The Gaussian part of the distribution corresponds, roughly, to the energy that would be reconstructed from an electron in the absence of bremsstrahlung. The tracker material varies quite strongly with η, and thus so does the amount of bremsstrahlung radiation, so one expects to see a variation in the fraction of events in the tail as a function of η, and this inevitably leads to some small variation in the peak position as a function of η.

We currently use corrections (“calibrations”) for the energy scale, designed to place the peak at 1.0, which are parameterized in terms of the number of crystals in the cluster ($f(N_{cry})$ corrections). This helps to minimize the residual dependence on both E and η of the energy scale. Figure 11 shows, as an example, E_{meas}/E_{true} as a function of the number of crystals in a reconstructed Hybrid super-cluster, for electrons $10 < p_T < 50$ GeV, together with a fitted polynomial function.

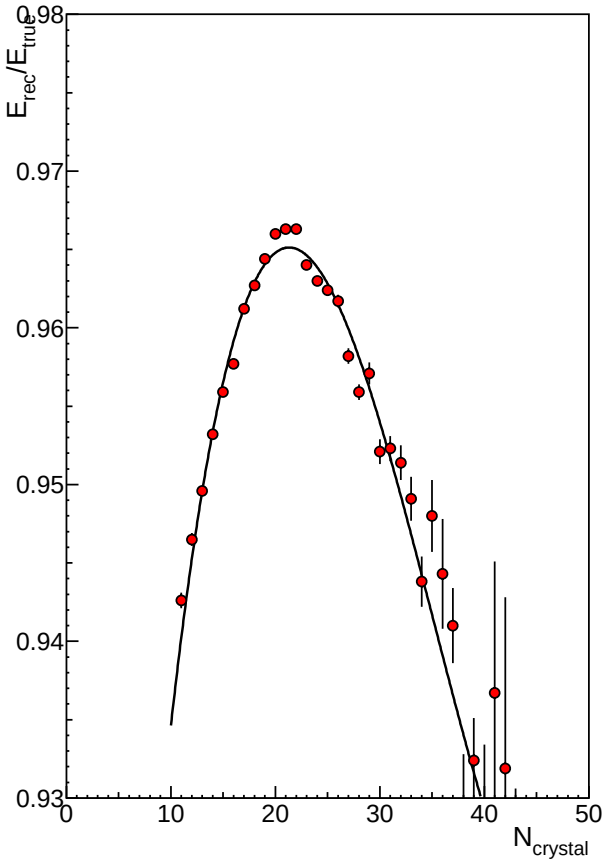

Fig. 11: E_{meas}/E_{true} as a function of the number of crystals in a Hybrid super-cluster, for electrons having a flat p_T spectrum in the range 10-50 GeV, together with a fitted polynomial function

Before the energy scale correction there is a non-linearity of the energy scale, a dependence of energy scale on E, as mentioned in the previous paragraph. This seems to be due to the zero suppression threshold applied in the simulated data production. Higher energy showers have more crystals above the fixed threshold. The effect is almost entirely removed by the $f(N_{cry})$ correction when using the Hybrid algorithm in the barrel.

In the endcap, where energy deposited in the preshower detector also needs to be included, the performance is not yet fully optimized. There are energy scale dependences on both η and E, even after a $f(N_{cry})$ correction. The reasons for the less good performance in the endcap, and, by implication, the steps necessary to remedy the situation have been discussed in section 7.

10 Energy and position measurement performance

The performance figures given in this section have been obtained using CMSIM/GEANT 3 simulation and CMS120 geometry (with one exception: the comparison with CMS116 results). The digitization was made with the EcalRealistic [9] digitization using default parameters. The additional smearings representing electronics noise, photostatistics and constant term contributions to the energy resolution, are also set to their default values: noise(barrel) 0.3 GeV, noise(endcap) 0.15 GeV,

constant term (intercalibration error and tolerance on longitudinal non-uniformity) 0.5%, and photostatistics contribution 4.0[7] photoelectrons/GeV.

For these performance figures an isolated Level-1 trigger is demanded, which results in a ~6% inefficiency mainly due to bremsstrahlung radiation in the isolation region, but *no trigger threshold is applied*. No plots or performance figures are given for the endcap region because the endcap reconstruction is still undergoing optimization, as discussed in a previous section.

Figure 12 shows the distribution of E_{meas}/E_{true} for 35 GeV electrons reconstructed using the Hybrid algorithm. The energy resolution is parametrized in two ways: in terms of the fitted width of the Gaussian part of the distribution (fitted between -1.5σ and $+2.0\sigma$), and in terms of σ_{eff}, defined as the half-width containing 68.3% of the distribution — if the distribution is Gaussian then σ_{eff} is just the Gaussian sigma, if the distribution has more significant tails then σ_{eff} provides some measure of this. The parameter σ_{eff} provides a convenient measure of performance which adequately reflects final physics performance (in extracting signal significance etc.). Figure 13 shows the position resolution in η and φ for the same sample. Table 2 collects together a more complete list of performance results for the Hybrid algorithm reconstructing electrons in the barrel. Values for $p_T = 35$ GeV photons are given, together with values for electrons having a flat p_T spectrum in the range $10 < p_T < 50$ GeV. Performance for the previous, CMS116, geometry with less tracker material, is included for comparison. It is perhaps worth noting, as a comparison, that unconverted photons with a flat p_T spectrum in the range $10 < p_T < 50$ GeV can be reconstructed, in the barrel using a 5x5 fixed window, and in the endcap using a 3x3 fixed window with impact position correction, achieving in both cases a resolution of $\sigma_{eff}/E = 0.9\%$.

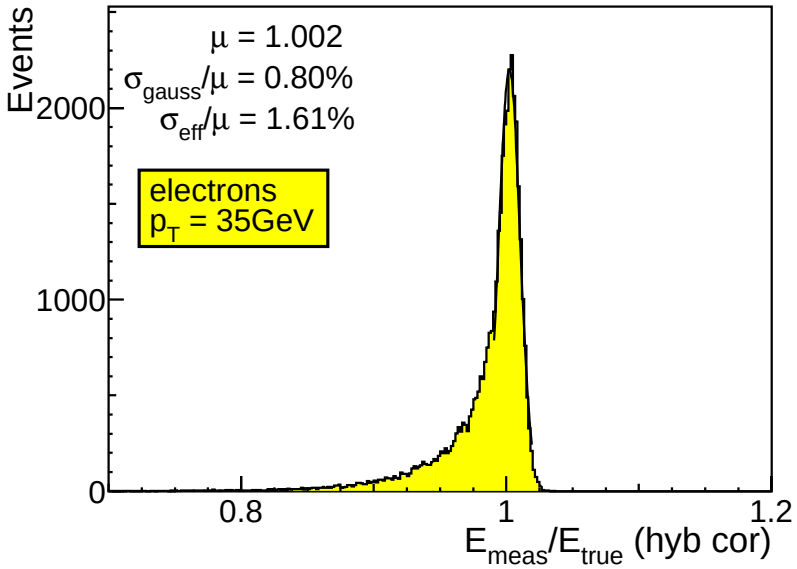

Fig. 12: Distribution of E_{meas}/E_{true} for 35 GeV electrons in the CMS barrel ECAL, simulated with CMS120 geometry, fully digitized without pileup, and reconstructed with the Hybrid super-clustering algorithm

7. There are a number of errors and imprecisions related to this number: its use in ORCA does not include the APD (or VPT) excess noise factor and the number for the endcap is not exactly that of the barrel, as well as the fact that the light output currently observed in the testbeam is closer to 6 p.e./GeV. However these imprecisions have very little impact on the results.
It is also to be noted that the 'constant term' of 0.5% per crystal is not quite the same as a constant term of 0.5% added to the energy resolution of a shower — although since most of the energy is usually contained in one or two crystals, the difference is not very large.

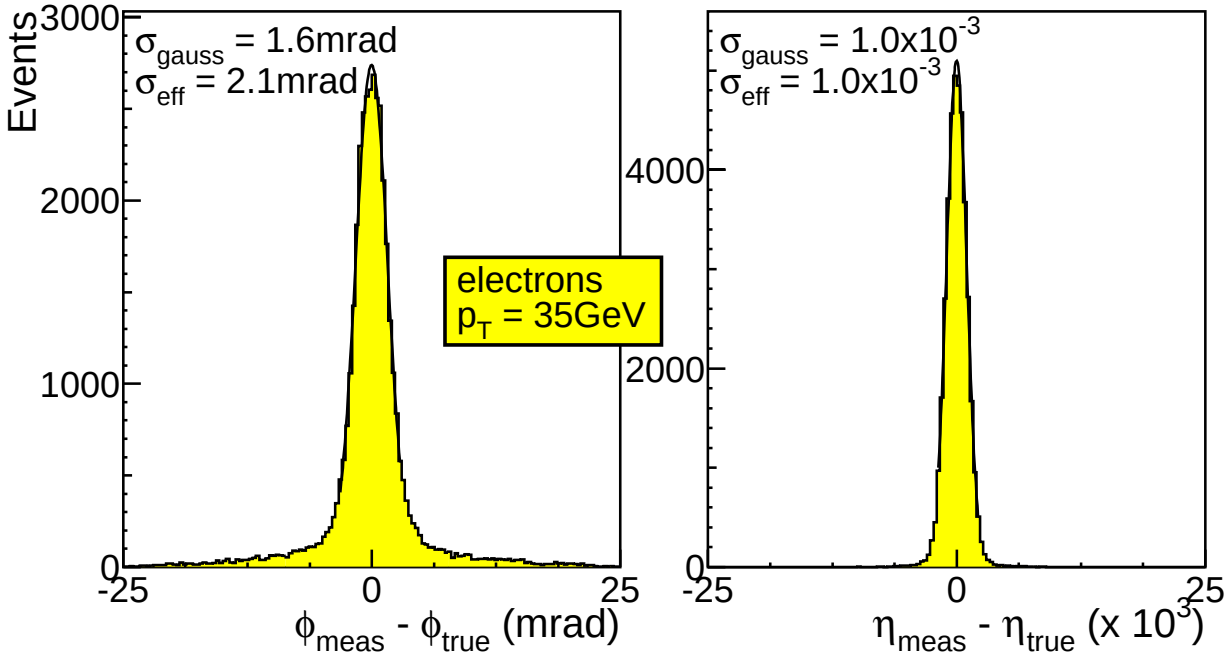

Fig. 13: Position resolution for 35 GeV electrons in the CMS barrel ECAL, simulated with CMS120 geometry, fully digitized without pileup, and reconstructed with the Hybrid super-clustering algorithm

Table 2: Performance of Hybrid super-clustering algorithm reconstructing electrons in the barrel ECAL

electron sample	**Energy resolution**		**Position resolution**			
	σ/E	**σ_{eff}/E**	**$\sigma(\eta)$**	**$\sigma_{eff}(\eta)$**	**$\sigma(\varphi)$**	**$\sigma_{eff}(\varphi)$**
p_T = 35 GeV	0.8%	1.6%	1.0 x 10^{-3}	1.0 x 10^{-3}	1.6mrad	2.1mrad
10 < p_T < 50 GeV	0.9%	2.1%	1.1 x 10^{-3}	1.1 x 10^{-3}	1.9mrad	2.6mrad
10 < p_T < 50 GeV (10^{34})	1.3%	2.7%	1.1 x 10^{-3}	1.1 x 10^{-3}	1.9mrad	3.0mrad
10 < p_T < 50 GeV (CMS116)	0.8%	1.5%	1.1 x 10^{-3}	1.1 x 10^{-3}	1.8mrad	2.1mrad

11 Acknowledgements

We gratefully acknowledge the help of many colleagues, both inside the ECAL-egamma group and in the wider field of the ORCA program development, and the Monte Carlo Data Production organization. Special mention should be made of Dave Barney, Edwige Tournefier and Aris Kyriakis for their work on endcap reconstruction.

12 References

[1] CMS ECAL Technical Design Report, CERN/LHCC 97-33, 15th Dec 1997

[2] GEANT3, version 3.21/13 (release 15111999), Detector Description and Simulation Tool, CERN program library long writeup W5013

[3] ORCA, Object-oriented Reconstruction for CMS Analysis — a CMS software program written in C++

[4] P. Aspell *et al.*, Results from the 1999 Beam Test of a Preshower Prototype, CMS-Note/ 2001-011

[5] This can be verified using longitudinal shower shape parameterizations — for example, using that of E. Longo and I. Sestili, Nucl. Instr. and Meth. **128** (1975), 283. (Quoted in Particle Data Group, Review of Particle Properties, Phys. Rev. **D 204** (1988) p66).

[6] See, for example, J.P. Peigneux et al., Results from Tests on Matrices of Lead Tungstate Crystals Using High Energy Beams, Nucl. Instrum. Methods, **A378** (1996) 410.

[7] T. C. Awes *et al.*, A Simple Method of Shower Localization and Identification in Laterally Segmented Calorimeters, Nucl. Instrum. Methods **A311**(1992), 130.

[8] I. Puljak, These de Doctorat de l'Universite Paris VI, 21 Sept 2000.

[9] For a description see: ORCA 4 - User Guide (http://cmsdoc.cern.ch/orca/Manuals/ UserGuide_ORCA_snapshot/html/). A description of the ECAL readout can be found in Appendix A of CMS Note 1999/024.